Title

Inter-organelle crosstalk supports acetyl-coenzyme A homeostasis and lipogenesis under metabolic stress

Short title**:** Peroxisomal metabolism supports acetyl-CoA homeostasis and lipid synthesis

Authors

Ramya S Kuna[1,2#], Avi Kumar[1,2#], Hector Galvez[1], Karl A Wessendorf-Rodriguez[1,2], Courtney R Green[1,2], Grace H McGregor[1,2], Thekla Cordes[1,2,4], Reuben J Shaw[1], Robert U Svensson[3], Christian M Metallo[1,2]*

Affiliations

[1] Department of Molecular and Cell Biology, Salk Institute for Biological Studies, La Jolla, CA 92037, USA

[2] Department of Bioengineering, University of California, San Diego, La Jolla, CA 92093, USA

[3]Nimbus Therapeutics, Cambridge, MA 02139, USA

[4]Department of Bioinformatics and Biochemistry, Braunschweig Integrated Centre of Systems Biology (BRICS), Technische Universität Braunschweig, Braunschweig 38106, Germany

# Ramya S Kuna and Avi Kumar contributed equally to this article.

*Corresponding author

Correspondence: metallo@salk.edu

Abstract

Proliferating cells rely on acetyl-CoA to support membrane biogenesis and acetylation. Several organelle-specific pathways are available for provision of acetyl-CoA as nutrient availability fluctuates, so understanding how cells maintain acetyl-CoA flux under such stresses is critically important. To this end we applied ^{13}C isotope tracing cell lines deficient in these mitochondrial (ATP-citrate lyase; ACLY-), cytosolic, (acetyl-CoA synthetase (ACSS2-), and peroxisomal (peroxisomal biogenesis factor 5; PEX5-) dependent pathways. ACLY knockout in multiple cell lines reduced fatty acid synthesis and increased reliance on extracellular lipids or acetate. Knockout of both ACLY and ACSS2 (DKO) severely stunted but did not entirely block proliferation, suggesting alternate pathways can support acetyl-CoA homeostasis. Metabolic tracing and PEX5 knockout studies link peroxisomal oxidation of exogenous lipids as a major source of acetyl-CoA for lipogenesis and histone acetylation, highlighting a role for inter-organelle crosstalk in supporting cell survival in response to nutrient fluctuations.

Teaser

We quantify how acetyl-CoA metabolism is supported by distinct pathways spanning mitochondria, cytosol, and peroxisomes using comprehensive tracing applied to knockout cells.

MAIN TEXT

Introduction

Acetyl-CoA is a critical precursor for acetylation and lipid synthesis associated with membrane biogenesis, energy storage, and protein modification (*1*). Central carbon metabolism is wired with several redundancies in place to maintain acetyl-CoA homeostasis under conditions of stress, with mitochondria, peroxisomes, and cytosolic acetate activation all contributing to this metabolic pool. While both healthy tissues and tumors readily incorporate lipids from the diet (*1*), *de novo* lipogenesis (*DNL*) is required for some tumors and cell types to proliferate (*2*, *3*), how each of these pathways and organelles fuel lipogenesis is not fully clear. Fatty acids are synthesized from two carbon acyl-units provided by cytosolic acetyl-CoA, which is metabolized to malonyl-CoA by acetyl-CoA Carboxylase (ACC) and used by fatty acid synthase (FASN) to generate long-chain fatty acids. These fatty acids can be further elongated, desaturated, and incorporated into lipids within the endoplasmic reticulum (ER). In the context of cancer, FASN inhibition reduces body weight (*4*), oncogene expression (*5*), and *in vivo* growth (*6*) of human breast cancer cell lines in mice. Knockout and pharmacological inhibition of acetyl-CoA carboxylase also compromise tumor growth in xenograft and genetically-engineered mouse models of lung cancer while synergizing with chemotherapy (*7*).

ATP-citrate lyase (ACLY) is the major conduit through which mitochondrial metabolism supports acetyl-CoA generation, which is important for lipid synthesis as well as epigenetic regulation and DNA repair via histone acetylation (*8–10*). Upregulation of ACLY expression has been identified in a number of numerous cancers upregulate ACLY expression compared to surrounding healthy tissue, including breast, liver, bladder, stomach, colorectal, glioblastoma, and lung cancers (*11–17*), and in patients with gastric adenocarcinoma (*18*) and lung adenocarcinomas (*17*), overexpression and activation of ACLY is associated with poor prognosis. Further, both pharmacological inhibition and genetic knockdown of ACLY have been demonstrated to reduce lipogenesis and cancer cell proliferation (*19–26*), supporting the link between ACLY activity and tumor growth. On the other hand, nutrient availability and mitochondrial metabolism are sometimes compromised in cells within the tumor microenvironment, and pathways like reductive carboxylation are often unable to fully compensate (*27*, *28*). Therefore, characterization of alternative acetyl-CoA sources may useful for understanding cancer cell survival and resistance mechanisms.

The acetyl-CoA synthetase family of enzymes (ACSS1, ACSS2, and ACSS3) are the rate limiting enzymes involved in acetate activation to acetyl-CoA in mammalian cells (*29*). While ACSS1 and ACSS3 are mitochondrially expressed and tissue-restricted (in the case of ACSS3), ACSS2 is localized in the cytosol (*30*). ACSS2 has garnered interest as a cancer target as high expression of ACSS2 is associated with poor prognosis in breast, glioblastoma, ovarian, and lung cancers (*31–33*). Nutrient deprivation, including hypoxia and lipid depletion, upregulate ACSS2 expression and acetate catabolism for DNL in cancer cells, suggesting that ACSS2 provides a mode of metabolic plasticity to cancer cells under stress (*34*). Hepatocyte selective depletion of ACSS2 or ACLY decreased liver acetyl-CoA levels in obese mice (*35*). Furthermore, mouse embryonic fibroblasts (MEFs) deficient in ACLY upregulate ACSS2 protein expression and increase utilization of acetate for cytosolic acetyl-CoA generation (*36*), highlighting the essentiality of acetyl-CoA and metabolic flexibility of proliferative cells.

Peroxisomes generate acetyl-CoA via β-oxidation of fatty acids, most often very long-chain (VLCFA) or branched-chain fatty acids (BCFA), which contribute to malonyl-CoA and lipids in the heart and liver (*37–40*). Peroxisomal enzymes involved in oxidation of branched chain fatty acids (HSD17B4, ACOX3) are overexpressed in cancerous prostate tissue compared to paired healthy tissue (*41*), suggesting this organelle may support generation of acetyl-CoA in tumors. However, the extent to which peroxisomal β-oxidation of fatty acids serves as a source of lipogenic acetyl-CoA in cancer cells under nutrient stress warrants further exploration.

Here we apply mass spectrometry, stable isotope tracing and isotopomer spectral analysis (ISA) to analyze the metabolic rewiring that occurs when acetyl-CoA synthesis is systematically compromised in cancer cells. We genetically engineered cancer cell lines deficient in ACLY and/or ACSS2 using CRISPR/Cas9. While knockout of ACLY decreased *DNL* under basal conditions, cells are able to sustain FASN flux and/or growth through use of exogenous acetate or serum lipids. On the other hand, knockout of both ACLY and ACSS2 induces a growth limiting stress regardless of medium nutrient status. Finally, we observe that ACLY-deficient cells use peroxisomal β-oxidation as a significant source of lipogenic acetyl-CoA and are sensitive to peroxisomal biogenesis factor 5 (PEX5) knockout or pharmacological inhibition of peroxisomal β-oxidation. Collectively, our study highlights the rewiring of organelle-specific acetyl-CoA metabolism in fueling DNL when mitochondrial (ACLY), cytosolic (ACSS2), and peroxisomal (PEX5) CoA sources are compromised in cancer cells.

Results

ACLY deficiency compromises fatty acid synthesis and drives lipid-dependence of cell lines

ACLY-knockout (*ACLY*-KO) clones were generated using CRISPR/Cas9 in A549 human NSCLC cells, 634T murine NSCLC cells, HepG2 hepatocarcinoma cells, and HAP1 cells (Fig. 1B, S1A). We observed increased protein expression of ACSS2 in the A549 and HepG2 *ACLY*-KO cell lines (Fig. 1B, S1A), consistent with previous results in MEFs (*36*). The growth rate of the *ACLY*-KO A549, 634T, and HAP1 cells was marginally lower compared to wildtype cells, while HepG2 *ACLY*-KO cells showed an over 50% reduction in growth rate compared to the wildtype cells (Fig. 1C, S1B). In A549 cells, *ACLY*-KO resulted in decreased glucose uptake/lactate secretion and increased glutamine uptake/glutamate secretion, suggesting rewiring of central carbon metabolism (Fig. 1D). To better understand how ACLY-deficiency alters intracellular metabolism, we cultured A549 clones in the presence of [U-$^{13}C_6$]glucose or [U-$^{13}C_5$]glutamine and quantified isotope enrichment in downstream metabolite pools. Enrichment of TCA cycle intermediates from glutamine in A549 *ACLY*-KO cells was elevated, consistent with extracellular flux results (Fig.1E). These findings may indicate that ACLY-KO induces oxidative stress, as increased glutamine catabolism has been found to be integral to maintaining redox homeostasis in cancer cells through multiple mechanisms (*42*, *43*). On the other hand, glucose enrichment in malate and aspartate (a readout of oxaloacetate) was increased, likely due to decreased generation of acetyl-CoA via ACLY and glutamine-dependent reductive carboxylation (Fig. S1C).

HepG2 cells express the plasma membrane citrate transporter SLC13A5 (*44*), so we next used [2,4-$^{13}C_2$]citrate to directly trace the ACLY reaction in HepG2 *ACLY*-KO cells, . Catabolism of [2,4-$^{13}C_2$]citrate provides insight into compartment-specific metabolism as M2 labeling of TCA intermediates will result from direct mitochondrial catabolism of labeled citrate, while M1 isotopologues will be formed if the tracer is first catabolized in the cytosol by ACLY (Fig. S1D). When culturing HepG2 wildtype and *ACLY*-KO cells in the presence of 500 μM [2,4-$^{13}C_2$]citrate, we found the ratio of M1/M2 labeling on malate, aspartate, succinate, and fumarate was significantly decreased in the *ACLY*-KO cells (Fig. S1E). Furthermore, the relative abundance of

M2 alpha-ketoglutarate was comparable to M1 labeling in wildtype cells but was significantly greater in the *ACLY*-KO cells (Fig. S1F). Additionally, enrichment of palmitate was minimal in the *ACLY*-KO cells compared to wildtype (Fig. S1G). These labeling patterns confirm that *ACLY*-KO forces cells to oxidize citrate in the mitochondria and/or cytosol to alpha-ketoglutarate at the expense of acetyl-CoA generation. Next, we applied ISA to quantify palmitate synthesis and the contribution of [U-$^{13}C_6$]glucose to the lipogenic acetyl-CoA pool. ACLY-deficiency profoundly decreased palmitate synthesis compared to control cells (Fig. 1F, S1H, I). Notably, *ACLY*-KO cells maintained some flux from [U-$^{13}C_6$]glucose to lipogenic acetyl-CoA such that ~20% of palmitate carbon was derived from glucose in A549 and HepG2 cells, while a smaller decrease was observed in 634T cells (Fig 1G, S1J). Collectively, these results indicate that ACLY deficiency effectively decreases FASN flux and alters cytosolic citrate shuttling under normal culture conditions while reducing growth slightly.

Acetate metabolism by ACSS2 supports lipogenesis to enable growth of ACLY-deficient cells

Under conditions where glucose-derived citrate is limiting, such as hypoxia, acetate can be "activated" by acetyl-CoA synthetase enzymes. As protein expression of ACSS2 was markedly increased in *ACLY*-KO cells (Fig. 1B, S1A), we hypothesized that acetate utilization may compensate for loss of ACLY. Supplementation of 1 mM [1,2-$^{13}C_2$]acetate to cultures significantly increased palmitate synthesis in cells lacking ACLY (Fig. 2A, S2A). Acetate became the primary lipogenic substrate in all tested *ACLY*-KO cell lines (Fig. 2B, S2B) but only contributed between 5-40% of lipogenic acetyl-CoA pools in control cells. *De novo* palmitate synthesis was significantly rescued in the *ACLY*-KO cells grown with acetate (Fig. 2A, S2A) compared to those grown in the absence of acetate (Fig. 1F, S1F,G) in all cell lines. We also measured the growth rate of control and ACLY-deficient cell lines in various culture media. *ACLY*-KO cells grew comparably to control cells in media supplemented with 10% dialyzed FBS (dFBS) (Fig 2C, S2C); however, when we removed serum lipids growth of all *ACLY*-KO cells was severely compromised (Fig 2C, S2C). Addition of 1 mM exogenous acetate enhanced the growth of all *ACLY*-KO cell lines while having no impact on growth rates of control cells (Fig 2C, S2C). The most dramatic growth impact of acetate was observed in cultures grown in delipidated serum (Fig 2C, S2C), highlighting the importance of this metabolic redundancy in supporting acetyl-CoA for lipid synthesis (Fig. 2D).

To confirm the role of ACSS2 in supporting lipogenesis, we examined the growth and metabolism of A549 and HepG2 cells lacking ACSS2 (Fig. 3A, S3A). While ACLY expression was unchanged in *ACSS2*-KO cells (Fig. 3A, S3A), the conversion of [1,2-$^{13}C_2$]acetate to palmitate was significantly decreased (Fig. 3B, S3B), and there was no impact on palmitate synthesis rates in cells lacking ACSS2 (Fig. 3C, S3C). Furthermore, the growth rates of both A549 and HepG2 cell lines were minimally impacted by *ACSS2*-KO in lipid-replete medium (Fig. 3D, S3D). However, HepG2 ACSS2-KO cells observed a significant growth defect compared to wildtype in lipid-depleted media (Fig S3D), matching previous studies which found ACSS2-KD was detrimental to cancer cell growth in conditions of metabolic stress (*31*, *34*). A549 ACSS2-KO cell growth remained unaffected by media delipidation (Fig. 3D). A similar phenotype bifurcation between the cell lines was observed previously, as HepG2 cells exhibited a greater growth rate reduction upon loss of ACLY compared to A549 cells (Fig. 1C, S1B). Interestingly, mRNA expression of ACSS1 and ACSS3, both mitochondrial isozymes of ACSS2, were significantly elevated in HepG2 hepatocarcinoma cells compared to A549 NSCLC cells (Fig. 3E). Furthermore, [1,2-$^{13}C_2$]acetate enrichment of TCA intermediates was significantly higher in HepG2 cells compared to A549 cells (Fig. 3F,G), suggesting that mitochondrial ACSS1 and/or ACSS3 compete with cytosolic ACSS2 for utilization of acetate and likely reflecting the metabolism in their tissues of origin. This metabolic redundancy may influence acetate shuttling to mitochondria, lipid pathways (e.g. ER),

193 and nucleus to impact epigenetic regulation which is altered by ACSS1/2 knockdown (*45*) but also
194 suggests this pathway may not be targetable in all tumor or cell types.
195
196 **Alternative pathways compensate for combined loss of ACLY and ACSS2**
197 Next we characterized A549 ACLY/ACSS2 double knockout (*ACLY/ACSS2*-DKO) cells to explore
198 how cancer cells respond to extreme restriction of acetyl-CoA sourcing (Fig. 4A). As expected,
199 growth of A549 *ACLY/ACSS2*-DKO cells was significantly impaired relative to wildtype in all
200 conditions tested, and we observed no rescue-effect with acetate supplementation (Fig 4B). We also
201 detected little to no isotope enrichment in palmitate from [U-$^{13}C_6$]glucose or [1,2-$^{13}C_2$]acetate in
202 *ACLY/ACSS2*-DKO cells (Fig. 4C, D), confirming that both pathways were defective in these cells.
203 Incorporation of polyunsaturated fatty acids (PUFA) into phosphatidylcholine (PC) lipids and
204 triacyl glycerides (TAG) was elevated in *ACLY*-KO and *ACLY/ACSS2*-DKO cells, indicating
205 increased reliance on exogenous fatty acids for membrane lipid synthesis in ACLY deficient cells
206 (Fig. 4E, S4A, B). PUFA-containing lipids drive sensitivity to lipid peroxidation (*46*), and we found
207 that PUFA-enriched *ACLY/ACSS2*-DKO cells were more susceptible to ferroptosis induced by
208 application of the glutathione peroxidase 4 (GPX4) inhibitor, ML210, than wildtype cells (Fig. 4F).
209 Despite these alterations in lipid metabolism, whole cell protein acetylation was maintained in lipid-
210 replete *ACLY*-KO and *ACLY/ACSS2*-DKO cells (Fig 4G, H), suggesting that NSCLC cells are able
211 to sustain acetyl-CoA availability through pathways independent of ACLY and ACSS2.
212
213 The continued availability of acetyl-CoA for histone acetylation suggests cancer cells can employ
214 alternate pathways for acetyl-CoA generation under conditions of metabolic stress, including non-
215 enzymatic mechanisms (*47*). To explore these pathways more deeply we cultured A549 *ACLY*-KO
216 and *ACLY/ACSS2*-DKO cells with either ^{13}C-labeled glucose, glutamine, and pyruvate for 72 hours
217 and quantified isotope enrichment in palmitate. In theory, knockout of ACLY will eliminate glucose
218 to palmitate carbon transfer (Fig. 5A); however, A549 *ACLY*-KO cells traced with [U-$^{13}C_6$]glucose
219 continued to sustain labeling on newly synthesized palmitate (Fig. 5B), and we observed similar
220 results with [3-^{13}C]pyruvate (Fig. 5C). Culture of the *ACLY*-KO and *ACLY/ACSS2*-DKO cells with
221 [U-$^{13}C_5$]glutamine yielded insignificant enrichment of palmitate (Fig. 5D), suggesting the existence
222 of a citrate/ACLY-independent lipogenic pathway which allows glucose and pyruvate but not
223 glutamine to generate acetyl-CoA. We previously demonstrated that carnitine acetyl-transferase
224 (CRAT) actively exports mitochondrial branched-chain-CoAs to enable their elongation to long-
225 chain monomethyl branched-chain fatty acids in adipocytes (*48*), and Izzo et al. have observed that
226 CRAT facilitates nuclear acetylation and lipogenesis (*49*). However, we hypothesize that this
227 activity is insufficient to support lipid synthesis since we observed minimal labeling of palmitate
228 from [U-$^{13}C_6$]glucose in the A549 *ACLY/ACSS2*-DKO (Fig. 5A), despite noting significant
229 enrichment of pyruvate and citrate (Fig. S5A,B). Likewise, ^{13}C pyruvate, and glutamine also
230 yielded negligible label on palmitate in A549 *ACLY/ACSS2*-DKO cells (Fig. 5B, C, D), suggesting
231 that ACSS2 is involved in the conversion of pyruvate to acetyl-CoA (Fig. 5A). Such a mechanism
232 has been described whereby reactive oxygen species facilitate oxidative decarboxylation of
233 pyruvate to acetate (*50*). The combination of KO cells and tracers applied here confirm this activity
234 supports acetyl-CoA generation, but the extracellular acetate, ACSS2, and lipid dependency of
235 *ACLY*-KO cell growth suggests this *de novo* acetate flux is not significant enough to sustain the
236 biosynthetic needs of the ACLY deficient cells tested here (Fig. 2C, S2C).
237
238 To examine how oxidation of fatty acyl-CoA might contribute to acetyl-CoA homeostasis we traced
239 the A549 cell panel with 500 μM [U-$^{13}C_8$]octanoate, which passively diffuses across the
240 mitochondrial membrane as well as peroxisomal membranes (*39*). Notably, octanoate contributed
241 significantly to fatty acid biosynthesis, even in *ACLY/ACSS2*-DKO cells (Fig. 5E,F, S5C) and
242 contrasting results with glucose, acetate, or glutamine tracers (Fig 4C, D, 5D). *ACLY*-KO and

ACLY/ACSS2-DKO cells had a 2.5-fold and 4-fold increase, respectively, in enrichment of the lipogenic acetyl-CoA pool from octanoate compared to the wildtype or *ACSS2*-KO cells (Fig. 5E). Similar trends in lipogenic acetyl-CoA labeling from [U-$^{13}C_8$]octanoate were observed in HepG2 and 634T *ACLY*-KO clones (Fig. S5C). Indeed, supplementation of octanoate enabled quantitation of fractional new fatty acid synthesis in *ACLY/ACSS2*-DKO cells by ISA (Fig. 5F). Citrate enrichment from octanoate was also increased in the *ACLY*-KO and *ACLY/ACSS2*-DKO cells (Fig. S5D). However, based on the previous [U-$^{13}C_5$]glutamine tracing results (Fig. 5D) mitochondrial citrate minimally contributes to fatty acid synthesis in the *ACLY*-KO or *ACLY/ACSS2*-DKO cells, and no carnitine was added to cultures(*49*), suggesting that ACLY-deficient cells use peroxisomal metabolism to supply acetyl-CoA for biosynthesis (Fig 5G).

Peroxisomal β-oxidation supplies lipogenic acetyl-CoA in the absence of ACLY and ACSS2

Peroxisomes are the site of β-oxidation for very long chain fatty acids (VLCFAs) and branched chain fatty acids (BCFAs). Peroxisomes are closely associated with lipid droplets and contain the metabolic machinery for acetyl-CoA generation from diverse fatty acids (*51*). In fact, Izzo et al. observed increased expression of peroxisomal fatty acid oxidation genes in their *ACLY/ACSS2*-DKO cell lines (*49*). To test whether peroxisomes could serve as an appreciable source of acetyl-CoA in cancer cells, we profiled lipid abundances in the A549 cell panel. While total TAGs were slightly reduced in most cells, total PCs were unchanged (Fig. 6A). However, we detected significant alterations in the acyl-chain composition of the lipids, such that TAGs and PCs containing VLCFAs were depleted in *ACLY*-KO and *ACLY/ACSS2*-DKO cells (Fig. 6B, C). This depletion is complete for nearly all measurable VLCFA containing saturated, mono-, and di-unsaturated TAG species (Fig. S6A) as well as saturated, and mono-unsaturated PC species (Fig S6B). Depletion of VLCFAs in lipids suggests altered VLCFA homeostasis, potentially due to increased VLCFA oxidation in the peroxisome or decreased elongation using acetyl-CoA.

To further investigate we studied role of peroxisomes in non-canonical lipogenic acetyl-CoA contribution. Peroxisome maintenance depends on the import of nuclear-encoded proteins containing a peroxisomal targeting signals (PTS1), which are recognized by cytosolic PEX5 receptors that transport them into the peroxisomal lumen. In the absence of PEX5 peroxisomal enzyme transport is ablated and metabolism altered (*52*). To further investigate the role of peroxisomes in supporting acetyl-CoA metabolism we generated *PEX5* and *ACLY/PEX5*-knockout (*ACLY/PEX5*-KO) clones using CRISPR/Cas9 in A549 cells (Fig. 6D). *ACLY/ACSS2/PEX5* triple knockout cells did not proliferate and could not be tested. We then cultured A549 *PEX5*-KO cells with 500 μM [U-$^{13}C_8$]octanoate and quantified its contribution to the lipogenic acetyl-CoA pool. Intriguingly, both enrichment from octanoate and fatty acid synthesis were significantly lower in *ACLY/PEX5*-KO cells compared to *ACLY*-KO cells (Fig 6E-F), providing evidence that peroxisomal metabolism supports acetyl-CoA and lipid synthesis. On the other hand, we saw no effect of PEX5 deficiency on lipogenic acetyl-CoA enrichment or palmitate synthesis in wildtype cells (Fig 6E-F). The labeling distribution of palmitate from [U-$^{13}C_8$]octanoate highlights these changes, as *ACLY*-KO cells showed robust incorporation but *ACLY/PEX5*-KO cells showing predominantly M8 palmitate (or direct incorporation of octanoate; Fig. S6C). These data suggest that knockout of PEX5 significantly disrupts the contribution of peroxisomal fatty acid oxidation to lipogenic acetyl-CoA production in the ACLY-KO cells (Fig 6G). In fact, we also observed a decrease in octanoate-mediated histone acetylation in *ACLY*/*PEX*5-KOs compared to *ACLY*-KO cells in delipidated media (Fig. S6D).

To elucidate how impairing peroxisomal β-oxidation affects proliferation of cells lacking ACLY, we quantified the growth of each cell line in response to knockout of *PEX5*. Strikingly, *ACLY/PEX5*-KO cells showed a significant decrease in growth relative to *ACLY*-KO cells, whereas

there was no growth effect on single *PEX5*-KO cells compared to wildtype (Fig. 6H). Finally, we quantified the growth the entire A549 ACLY/ACSS2-KO cell panel in response to increasing concentrations of the peroxisomal β-oxidation inhibitor, Thioridazine (Thio) (*53*, *54*) (Fig 6I). Strikingly, *ACLY*-KO and *ACLY/ACSS2*-DKO cells were significantly more sensitive to Thio treatment than wildtype or *ACSS2*-KO cells (Fig. 6J). Application of 2.5 μM Thio had no appreciable impact on growth of wildtype and *ACSS2*-KO cells, but significantly decreased proliferation of *ACLY*-KO and *ACLY/ACSS2*-DKO cells (Fig. 6I). Together, these results suggest that peroxisomal β-oxidation provides a significant growth sustaining level of acetyl-CoA in the absence of functional ACLY. Multiple mechanisms have been suggested for shuttling peroxisomal acetyl-CoA to the cytosol in mammalian cells, including conversion to acetate by a thioesterase and subsequent export (and activation by ACSS2 in the cytosol) as well as shuttling as acetyl-carnitine facilitated by peroxisomal CRAT (*55–57*). The elevated palmitate enrichment from [U-$^{13}C_8$]octanoate observed in *ACLY/ACSS2*-DKO cells suggests that these cells employ an acetate-independent acetyl-CoA export mechanism, potentially via activity of peroxisomal CRAT (Fig. 6G), which is also localized to mitochondria.

Discussion

While the core metabolic machinery of cancer cells acts "as advertised" under nutrient replete conditions, the diverse stresses experienced the tumor microenvironment induce complex rewiring of metabolic fluxes between organelles, including mitochondria, the ER, peroxisomes, and the plasma membrane. Here we show this organelle crosstalk is critical for cancer cells to maintain acetyl-CoA homeostasis and metabolic resilience when organelle-specific pathways become compromised. Acetyl-CoA serves as a substrate regulating numerous processes across mitochondria, the nucleus, peroxisomes, the ER, and plasma membrane but importantly cannot cross membranes. As such, understanding how acetyl-groups are shuttled throughout the cell for bioenergetics, biosynthesis, and cellular regulation is critically important. Here we applied metabolic tracing and lipogenesis studies to cancer cell lines where key pathways for acetyl-CoA generation were knocked out, including ACLY, ACSS2, and peroxisomal metabolism (PEX5). We further highlight a key role for peroxisomal metabolism in providing acetyl-CoA for fatty acid synthesis and histone acetylation.

Acetyl-CoA-fueled fatty acid synthesis is important for cancer progression in NSCLC models, whether this occurs in endogenous tissues or in situ within tumors (*7*). Targeting of ACLY to reduce tumor cell growth and increase dependence on exogenous lipids has also been explored in detail (*24–26*, *58*). Likewise, ACSS2 has garnered significant interest as a mechanism through which cancer cells source acetyl-CoA for growth and survival (*31–33*, *59*). ACSS2 expression and acetate-dependent flux both increase in the context of ACLY deficiency (*36*), and trafficking of acetate to the nucleus for histone acetylation may be an important aspect of this enzyme's function (*45*, *60–62*). The impact of ACSS isozyme expression on acetate shuttling, fatty acid synthesis and epigenetic regulation warrants further study as it may provide insight into how therapeutic interventions targeting acetate catabolism impact whole body physiology. Peroxisomes further complicate these questions, particularly in reference to their impact on lipid homeostasis and diversity. Understanding how these nodes of metabolic exchange are exploited by cancer cells shed light on resistance mechanisms, as these redundancies in pathway architecture can reduce efficacy of drugs targeting metabolic enzymes (*63*).

Beyond cancer, understanding how cells manage intracellular metabolic pools using these KO and tracing approaches is also relevant for states of "overnutrition." Indeed, exogenous treatment of fatty acids or lipids to cells in vitro often occurs at supra-physiological levels, so our studies further

343 highlight the role of peroxisomal metabolism in generating acetyl-CoA for lipid biosynthesis and
344 acetylation (*51*). While these KO systems lack some physiology in the acute nature of pathway
345 targeting, they also allow one to focus biochemical studies on these alternate pathways when
346 substrate levels are high. However, we and Luke Izzo et al(*49*). in this issue also note key questions
347 that remain such as the relative contribution of mitochondrial versus peroxisomal oxidation and the
348 dependence on carnitine for transport since both organelles express CRAT (*64*, *65*). The relative
349 contribution of each pathway likely shifts as a function of cell and tissue type, and these pathways
350 may also be distinct with respect to how they contribute to downstream lipid synthesis versus
351 histone acetylation. By understanding how these metabolic pathways are balanced they can be more
352 effectively targeted both in neoplastic or metabolically stressed tissues.
353
354 **Materials and Methods**
355
356 **Cell Lines**
357 A549 and HepG2 cells were obtained from HDBiosciences, HAP1 cells were obtained from
358 Horizon Discovery, and 634T cells were obtained from the Shaw Lab at the Salk Institute for
359 Biological Sciences. All cell lines were incubated at 37C with 5% CO_2 and cultured using
360 Dulbecco's Modified Eagle Media (DMEM) with 10% Fetal Bovine Serum and 1% Penicillin-
361 Streptomycin. Cells tested negative for mycoplasma contamination. All media were adjusted to pH
362 = 7.3.
363
364 **Cell Proliferation and ^{13}C Tracing**
365 Proliferation studies were performed on 12 well plates with an initial cell number of 50,000/well
366 for A549s and 100,000/well for HepG2s. Cells were plated in growth media and allowed to adhere
367 for 24 hours before changing to the specified growth media. Cell counts were performed at days 0
368 and 4 using a hemocytometer.
369
370 ^{13}C isotope tracing media was formulated using glucose and glutamine free DMEM 5030
371 supplemented with either 20 mM [U-$^{13}C_6$]glucose, 4 mM [U-$^{13}C_5$]glutamine, 1 mM [1,2-
372 $^{13}C_2$]acetate, 5 mM [3-$^{13}C_1$]pyruvate, 500 µM [U-$^{13}C_8$] octanoate or 500 µM [2,4-$^{13}C_2$]citrate
373 (Cambridge Isotopes) and 10% dialyzed FBS. ^{13}C palmitate studies were performed with 200 µM
374 albumin conjugated [U-$^{13}C_{16}$] palmitate and 10% dialyzed delipidated FBS. All studies were
375 performed with a final concentration of 20 mM glucose and 4 mM glutamine. Cultured cells were
376 washed with 1 mL PBS prior to applying tracing media for 6-72 hours as indicated in figure legends.
377
378 **Drug Dose Response**
379 Drug dose response studies were performed on 96 well plates with an initial cell number of
380 2,500/well. Cells were plated in growth media and allowed to adhere for 24 hours before changing
381 to the specified growth media with the indicated concentration of thioridazine. After 4 days wells
382 were washed 2x with tap water, 50uL of 0.5% crystal violet staining solution were added to each
383 well for 20 minutes. Crystal violet stain was removed and wells were washed 3x with tap water and
384 air dried overnight. Next, 200 uL methanol was added to each well and plates were incubated at
385 room temperature for 20 minutes. Optical density of wells were measured at 570 nm on a TECAN
386 plate reader.
387
388 **Ferroptosis Assay**
389 Wildtype and ACLY/ACSS2-DKO cells were plated in 96 well plates with an initial cell number
390 of 5,000/well. Cells were plated in growth media and allowed to adhere for 24 hours before
391 changing to the specified growth media with 2uM ML210 and/or 6uM Ferrostatin. After 48 hours,

392 cell viability was quantified using the PrestoBlue™ Cell Viability (Thermo, A13261) and a TECAN
393 plate reader.
394
395 **Isotopomer Spectral Analysis (ISA)**
396 Isotopomer spectral analysis (ISA) was performed to estimate the percent of newly synthesized
397 palmitate as well as the contribution of a tracer of interest to the lipogenic acetyl-CoA pool (*66*,
398 *67*). Parameters for contribution of ^{13}C tracers to lipogenic acetyl-CoA (D value) and percentage of
399 newly synthesized fatty acid (g(t) value) and their 95% confidence intervals are then calculated
400 using best-fit model from INCA MFA software. Experimental palmitate labeling from [U-
401 $^{13}C_6$]glucose, [U-$^{13}C_5$]glutamine, [1,2-$^{13}C_2$]acetate, [U-$^{13}C_8$] octanoate or [2,4-$^{13}C_2$]citrate after a
402 24-72 hour trace, as indicated in figure legends, was compared to simulated labeling using a reaction
403 network where C16:0 is condensation of 8 AcCoA. ISA data plotted as mean ± 95% CI. * indicates
404 statistical significance by non-overlapping confidence intervals.
405
406 **CRISPR/cas9 engineered knockout cell lines**
407 HDBiosciences generated A549 and HepG2 *ACLY*-KO, *ACSS2*-KO, and *ACLY/ACSS2*-DKO cell
408 lines. *ACLY, ACSS2,* and *ACLY/ACSS2* knockout clones were generated using the strategy
409 described previously (*68*). Briefly, a tandem guide RNAs (gRNAs) was designed to target the
410 human *ACLY* (gRNA sequences: gaccagctgatcaaacgtcg, ggggtcaggatgaacgtgtg) and *ACSS2* (gRNA
411 sequences: ctcgcggtagcgctgcagcg, aatggaaaagggattccggg) using the online CRISPR guide tool
412 provided by the Zhang Lab at MIT (http://tools.genome-engineering.org). The gRNA duplex was
413 cloned into lentiCRISPRv2 (Addgene #52961) (*69*). A549 and HepG2 cells were transfected with
414 the *ACLY* and/or *ACSS2* specific gRNA to generate pooled knockouts. After puromycin selection,
415 single-cell clones were isolated by diluting the pooled knockout lines at 1 cell/100 µL and plating
416 100 µL into each well of a 96 well plate. Clones were maintained by exchanging media every 3-5
417 days. Clones were validated by PCR and western blot. PEX5 and ACLY/PEX5 knockout clones
418 were generated using the strategy described previously (*70*). Briefly, chemically modified guide
419 RNAs (gRNAs) (Synthego) were designed to target the human PEX5 (gRNA sequences:
420 guugguggcugaauucc). gRNAs were complexed with recombinant Cas9 (IDT Cat#1081059) and
421 introduced into cells by electroporation (4D-Nucleofector, Lonza Biosciences) according to
422 manufacturer protocols. Single cell clones were generated by serial dilution of the bulk knockout
423 population in 96 well plates. Clones were maintained by exchanging the media every 3 days and
424 validated by western blot.
425
426 **Lentivirus Production**
427 One 10cm dish of HEK293FT cells at 60% confluency were transfected with 1.3 µg
428 VSV.G/pMD2.G, 5.3 µg lenti-gag/pol/pCMVR8.2, and 4 µg of the gRNA duplexed
429 lentiCRISPRv2 using 16 µL Lipofectamine 3000 diluted in 0.66 mL of OPTI-MEM. Medium
430 containing viral particles was harvested 48 and 72 hours after transfection, then concentrated by
431 Centricon Plus-20 100,000 NMWL centrifugal ultrafilters, divided into aliquots and frozen at -
432 80°C.
433
434 **Metabolic Flux Analysis**
435 Metabolic fluxes for citrate were calculated by collecting media at time 0 and spent media after 72
436 hours. Spent media was centrifuged at 300g for 5 min, to remove cell debris. Cell counts were
437 performed at time 0 and after 72 hours as well.
438
439 **Metabolite Extraction and GC-MS Analysis**
440 At the conclusion of the tracer experiment, media was aspirated. Then, cells were rinsed twice with
441 0.9% saline solution and lysed with 250 µL ice-cold methanol. After 1 minute, 100 µL water

442 containing 1 µg/ml norvaline was added to each sample and vortexed for one minute. 250 µL
443 chloroform was added to each sample, and all were vortexed again for 1 minute. After
444 centrifugation at 21,130 g for 10 minutes at 4°C, 250 µL of the upper aqueous layer was collected
445 and evaporated under vacuum at 4°C. Then, 250 µL of the lower organic layer was collected and
446 evaporated under air at room temperature. Dried polar and nonpolar metabolites were processed for
447 gas chromatography (GC) mass spectrometry (MS) as described previously in Cordes and Metallo
448 (*67*). Briefly, polar metabolites were derivatized using a Gerstel MultiPurpose Sampler (MPS 2XL).
449 Methoxime-tBDMS derivatives were formed by addition of 15 µL 2% (w/v) methoxylamine
450 hydrochloride (MP Biomedicals, Solon, OH) in pyridine and incubated at 45°C for 60 minutes.
451 Samples were then silylated by addition of 15 µL of N-tert-butyldimethylsily-N-
452 methyltrifluoroacetamide (MTBSTFA) with 1% tert-butyldimethylchlorosilane (tBDMS) (Regis
453 Technologies, Morton Grove, IL) and incubated at 45°C for 30 minutes. Nonpolar metabolites were
454 saponified and transesterified to fatty acid methyl esters (FAMEs) by adding 500 µL of 2% H_2SO_4
455 in methanol to the dried nonpolar layer and heating at 50°C for 1 hour. FAMEs were then extracted
456 by adding 100 µL of a saturated salt solution and 500 µL hexane and vortexing for 1 minute. The
457 hexane layer was removed, evaporated, and resuspended with 60µL hexane for injection.
458
459 Derivatized polar samples were injected into a GC-MS using a DB-35MS column (30m x 0.25mm
460 i.d. x 0.25µm, Agilent J&W Scientific, Santa Clara, CA) installed in an Agilent 7890B GC system
461 integrated with an Agilent 5977a MS. Samples were injected at a GC oven temperature of 100°C
462 which was held for 1 minute before ramping to 255°C at 3.5°C/min then to 320°C at 15°C/min and
463 held for 3 minutes. Electron impact ionization was performed with the MS scanning over the range
464 of 100-650 m/z for polar metabolites.
465
466 Derivatized nonpolar samples were injected into a GC-MS using a Fame Select column (100m x
467 0.25mm i.d. x 0.25µm, Agilent J&W Scientific, Santa Clara, CA) installed in an Agilent 7890A GC
468 system integrated with an Agilent 5977A MS. Samples were injected at a GC oven temperature of
469 80°C which was held for 1 minute before ramping to 170°C at 20°C/min then to 188°C at 1°C/min
470 then to 250°C at 20°C/min and held for 10 minutes. Electron impact ionization was performed with
471 the MS scanning over the range of 54-400 m/z for nonpolar metabolites.
472 Metabolite levels and mass isotopomer distributions were analyzed with an in-house Matlab script
473 which integrated the metabolite fragment ions and corrected for natural isotope abundances. Mole
474 percent enrichment calculations were performed using Escher-Trace (*71*).
475
476 **LC-MS/MS analysis**
477 Lipids were extracted from confluent 6 well plates after growth in DMEM + 10% FBS + 1%
478 penicillin streptomycin for 48 hours. At the conclusion of the experiment, media was aspirated, and
479 the cells were rinsed twice with saline solution. Cells were lysed with 750 µL of ice cold 1:1
480 methanol/water solution for 5 minutes on ice and scraped into Eppendorf tubes. Next, 500 µL of
481 ice cold chloroform and 50 uL butylated hydroxytoluene (1mg/mL in methanol) were added to the
482 tube, along with EquiSLASH (Avanti, Croda International Plc, 330731internal standard. The tubes
483 were vortexed for 5 min and centrifuged at 21,230g at 4°C for 5 min. The lower organic phase was
484 collected and 2 µL of formic acid was added to the remaining polar phase which was re-extracted
485 with 500uL of chloroform. Combined organic phases were dried under nitrogen and the pellet was
486 resuspended in 50 µL isopropyl alcohol.
487
488 Q Exactive orbitrap mass spectrometer with a Vanquish Flex Binary UHPLC system (Thermo
489 Scientific) was used with an Accucore C30, 150 x 2.1mm, 2.6 µm particle (Thermo) column at
490 40°C. 5 µL of sample was injected. Chromatography was performed using a gradient of 40:60 v/v
491 water: acetonitrile with 10 mM ammonium formate and 0.1% formic acid (mobile phase A) and

10:90 v/v acetonitrile: 2-propanol with 10 mM ammonium formate and 0.1% formic acid (mobile phase B), both at a flow rate of 0.2 mL/min. The LC gradient ran from 30% to 43% B from 3-8 min, then from 43% to 50% B from 8-9min, then 50-90% B from 9-18min, then 90-99% B from 18-26 min, then held at 99% B from 26-30min, before returning to 30% B in 6 min and held for a further 4 min.

Lipids were analyzed in positive mode using spray voltage 3.2 kV. Sweep gas flow was 1 arbitrary units, auxiliary gas flow 2 arbitrary units and sheath gas flow 40 arbitrary units, with a capillary temperature of 325°C. Full MS (scan range 200-2000 m/z) was used at 70 000 resolution with 1e6 automatic gain control and a maximum injection time of 100 ms. Data dependent MS2 (Top 6) mode at 17 500 resolution with automatic gain control set at 1e5 with a maximum injection time of 50 ms was used. Data was analyzed using EI-Maven and Escher-Trace software, and peaks normalized to Avanti EquiSPLASH internal standard. Lipid species specific fragments used for identification and quantitation are presented in the Supplementary Table 1

Western Blot

A549, HepG2, HAP1, and 634T wildtype, ACLY and/or ACSS2-KO cell lines were lysed in M-PER buffer (Thermo Scientific, 78501) with 1x protease inhibitor (Sigma-Aldrich). Protein concentrations were determined using Pierce™ BCA protein assay kit (Thermo Scientific, 23225). 15 ug protein were loaded and separated using 4–15% Mini-PROTEAN® TGX™ Precast SDS-PAGE Gels (Bio-rad, #4561086). Samples were then transferred to nitrocellulose membranes for immunoblotting. Total acetylated-lysine (Cell Signaling Technology, 9441), β-Actin (Sigma, A5441), ACLY (Cell Signaling Technology, 13390), and ACSS2 (Cell Signaling Technology, 3658), PEX5(D7V4D) (Cell Signaling Technology, 83020) antibodies were used to probe their respective targets. Anti-Rabbit horseradish peroxidase-conjugated secondary antibodies (Millipore, AP132P) were used for imaging.

RNA isolation and quantitative RT-PCR

Total RNA was purified from cultured cells using Trizol Reagent (Life Technologies) per manufacturer's instructions. First-strand cDNA was synthesized from 1 µg of total RNA using iScript Reverse Transcription Supermix for RT-PCR (Bio-Rad Laboratories) according to the manufacturer's instructions. Individual 20 µl SYBR Green real-time PCR reactions consisted of 1 µl of diluted cDNA, 10 µl of SYBR Green Supermix (Bio-Rad), and 1 µl of each 5 µM forward and reverse primers. For standardization of quantification, 18S was amplified simultaneously. The PCR was carried out on 96-well plates on a CFX Connect Real time System (Bio-Rad), using a three-stage program provided by the manufacturer: 95 °C for 3 min, 40 cycles of 95 °C for 10 s and 60 °C for 30 s. Gene-specific primers are tabulated in Table S1.

Quantification and Statistical Analysis

Statistical analyses were performed using Graphpad PRISM. Unless indicated, all results shown as mean ± SD of cellular triplicates obtained from one representative experiment as specified in each figure legend. P values were calculated using a Student's two-tailed *t* test, One-way ANOVA w/ Dunnet's method for multiple comparisons, or Two-way ANOVA w/ Tukey's method for multiple comparisons; *, P value < 0.05; **, P value < 0.01; ***, P value < 0.001, ****, P value < 0.0001. Unless indicated, all normalization and statistical tests compared to wildtype cells.

References

1. J. A. Menendez, R. Lupu, Fatty acid synthase and the lipogenic phenotype in cancer pathogenesis. *Nat. Rev. Cancer*. **7** (2007), doi:10.1038/nrc2222.
2. Y. Cai, J. Crowther, T. Pastor, J. Dehairs, J. V Swinnen, A. A. Sablina, Loss of Chromosome 8p Governs Tumor Progression and Drug Response by Altering Lipid Metabolism Article Loss of Chromosome 8p Governs Tumor Progression and Drug Response by Altering Lipid Metabolism. *Cancer Cell*. **29**, 751–766 (2016).
3. M. Knobloch, S. M. G. Braun, L. Zurkirchen, C. Von Schoultz, N. Zamboni, M. J. Arauzo-bravo, W. J. Kovacs, Ö. Karalay, R. A. C. Machado, M. Roccio, M. P. Lutolf, C. F. Semenkovich, S. Jessberger, Metabolic control of adult neural stem cell activity by Fasn-dependent lipogenesis. *Nature*. **493**, 226–230 (2014).
4. T. M. Loftus, D. E. Jaworsky, G. L. Frehywot, C. A. Townsend, G. V Ronnett, M. D. Lane, F. P. Kuhajda, Reduced Food Intake and Body Weight in Mice Treated with Fatty Acid Synthase Inhibitors. *Science (80-.).* **288**, 2379–2382 (2000).
5. J. A. Menendez, L. Vellon, I. Mehmi, B. P. Oza, S. Ropero, R. Colomer, R. Lupu, Inhibition of fatty acid synthase (FAS) suppresses HER2/neu (erbB-2) oncogene overexpression in cancer cells. *Proc. Natl. Acad. Sci.* **101**, 10715–10720 (2004).
6. E. S. Pizer, J. Thupari, W. F. Han, M. L. Pinn, F. J. Chrest, G. L. Frehywot, C. A. Townsend, F. P. Kuhajda, Malonyl-Coenzyme-A Is a Potential Mediator of Cytotoxicity Induced by Fatty-Acid Synthase Inhibition in Human Breast Cancer Cells and Xenografts 1. *Cancer Res.* **60**, 213–218 (2000).
7. R. U. Svensson, S. J. Parker, L. J. Eichner, M. J. Kolar, M. Wallace, S. N. Brun, P. S. Lombardo, J. L. Van Nostrand, A. Hutchins, L. Vera, L. Gerken, J. Greenwood, S. Bhat, G. Harriman, W. F. Westlin, H. J. Harwood, A. Saghatelian, R. Kapeller, C. M. Metallo, R. J. Shaw, Inhibition of acetyl-CoA carboxylase suppresses fatty acid synthesis and tumor growth of non-small-cell lung cancer in preclinical models. *Nat. Med.* **22**, 1108–1119 (2016).
8. K. E. Wellen, G. Hatzivassiliou, U. M. Sachdeva, T. V Bui, J. R. Cross, C. B. Thompson, ATP-Citrate Lyase Links Cellular Metabolism to Histone Acetylation. *Science (80-.).* **324**, 1076–1080 (2009).
9. J. V Lee, A. Carrer, S. Shah, N. W. Snyder, S. Wei, S. Venneti, A. J. Worth, Z. F. Yuan, H. W. Lim, S. Liu, E. Jackson, N. M. Aiello, N. B. Haas, T. R. Rebbeck, A. Judkins, K. J. Won, L. A. Chodosh, B. A. Garcia, B. Z. Stanger, M. D. Feldman, I. A. Blair, K. E. Wellen, Akt-dependent metabolic reprogramming regulates tumor cell Histone acetylation. *Cell Metab.* **20**, 306–319 (2014).
10. S. Sivanand, S. Rhoades, Q. Jiang, J. V Lee, J. Benci, J. Zhang, S. Yuan, I. Viney, S. Zhao, A. Carrer, M. J. Bennett, A. J. Minn, A. M. Weljie, R. A. Greenberg, K. E. Wellen, Nuclear Acetyl-CoA Production by ACLY Promotes Homologous Recombination. *Mol. Cell*. **67**, 252--265.e6 (2017).
11. H. F. Yancy, J. A. Mason, S. Peters, C. E. T. Iii, G. K. Littleton, M. Jett, A. A. Day, Metastatic progression and gene expression between breast cancer cell lines from African American and Caucasian women. *J. Carcinog.* **6** (2007), doi:10.1186/1477-3163-6-8.
12. E. D. Pope, E. O. Kimbrough, L. P. Vemireddy, P. K. Surapaneni, J. A. Copland, K. Mody, Aberrant lipid metabolism as a therapeutic target in liver cancer. *Expert Opin. Ther. Targets*. **23**, 473–483 (2019).
13. J. Turyn, B. Schlichtholz, A. Dettlaff-Pokora, M. Presler, E. Goyke, M. Matuszewski, Z. Kmieć, K. Krajka, J. Swierczynski, Increased Activity of Glycerol 3-phosphate Dehydrogenase and Other Lipogenic Enzymes in Human Bladder Cancer. *Horm. Metab. Res.* **35**, 565–569 (2003).

590 14. A. Varis, M. Wolf, O. Monni, M. Vakkari, A. Kokkola, C. Moskaluk, H. Frierson, S. M.
591 Powell, S. Knuutila, A. Kallioniemi, W. El-rifai, Targets of Gene Amplification and
592 Overexpression at 17q in Gastric Cancer 1. *Cancer Res.* **62**, 2625–2629 (2002).
593 15. Y. Zhou, L. R. Bollu, F. Tozzi, X. Ye, R. Bhattacharya, G. Gao, E. Dupre, L. Xia, J. Lu, F.
594 Fan, S. Bellister, L. M. Ellis, Z. Weihua, ATP citrate lyase mediates resistance of
595 colorectal cancer cells to SN38. *Mol. Cancer Ther.* **12**, 2782–2791 (2013).
596 16. M. E. Beckner, W. Fellows-Mayle, Z. Zhang, N. R. Agostino, J. A. Kant, B. W. Day, I. F.
597 Pollack, Identification of ATP Citrate Lyase as a Positive Regulator of Glycolytic Function
598 in Glioblastomas. *Int. J. Cancer*. **126**, 2282–2295 (2011).
599 17. T. Migita, T. Narita, K. Nomura, E. Miyagi, F. Inazuka, M. Matsuura, M. Ushijima, T.
600 Mashima, H. Seimiya, Y. Satoh, S. Okumura, K. Nakagawa, Y. Ishikawa, ATP Citrate
601 Lyase : Activation and Therapeutic Implications in Non–Small Cell Lung Cancer. *Cancer*
602 *Res.* **68**, 8547–8555 (2008).
603 18. X. Qian, J. Hu, J. Zhao, H. Chen, ATP citrate lyase expression is associated with advanced
604 stage and prognosis in gastric adenocarcinoma. *Int. J. Clin. Exp. Med.* **8**, 7855–7860
605 (2015).
606 19. C. Sullivan, J. G. Hamilton, R. Wheatley, C. River, B. Laboratories, Inhibition of
607 Lipogenesis in Rat Liver by (-)Hydroxycitrate. *Arch. Biochem. Biophys.* **150**, 183–190
608 (1972).
609 20. J. M. Lowenstein, Effect of (-)Hydroxycitrate on Fatty Acid Synthesis by Rat Liver in
610 Vivo. *J. Biol. Chem.* **246**, 629–632 (1971).
611 21. S. L. Pinkosky, S. Filippov, R. A. K. Srivastava, J. C. Hanselman, C. D. Bradshaw, T. R.
612 Hurley, C. T. Cramer, M. A. Spahr, A. F. Brant, J. L. Houghton, C. Baker, M. Naples, K.
613 Adeli, R. S. Newton, AMP-activated protein kinase and ATP-citrate lyase are two distinct
614 molecular targets for ETC-1002, a novel small molecule regulator of lipid and
615 carbohydrate metabolism. *J. Lipid Res.* **54**, 134–151 (2013).
616 22. D. E. Bauer, G. Hatzivassiliou, F. Zhao, C. Andreadis, C. B. Thompson, ATP citrate lyase
617 is an important component of cell growth and transformation. *Oncogene*. **24**, 6314–6322
618 (2005).
619 23. K. S. Lucenay, I. Doostan, C. Karakas, T. Bui, Z. Ding, G. B. Mills, K. K. Hunt, K.
620 Keyomarsi, Cyclin E Associates with the Lipogenic Enzyme ATP-Citrate Lyase to Enable
621 Malignant Growth of Breast Cancer Cells. *Cancer Res.* **76**, 2406–2419 (2016).
622 24. N. Zaidi, I. Royaux, J. V Swinnen, K. Smans, ATP Citrate Lyase Knockdown Induces
623 Growth Arrest and Apoptosis through Different Cell- and Environment- Dependent
624 Mechanisms. *Mol. Cancer Ther.* **11**, 1925–1936 (2012).
625 25. G. Hatzivassiliou, F. Zhao, D. E. Bauer, C. Andreadis, A. N. Shaw, D. Dhanak, S. R.
626 Hingorani, D. A. Tuveson, C. B. Thompson, ATP citrate lyase inhibition can suppress
627 tumor cell growth. *Cancer Cell*. **8**, 311–321 (2005).
628 26. D. Wang, L. Yin, J. Wei, Z. Yang, ATP citrate lyase is increased in human breast cancer ,
629 depletion of which promotes apoptosis. *Tumor Biol.* (2017),
630 doi:10.1177/1010428317698338.
631 27. C. M. Metallo, P. A. Gameiro, E. L. Bell, K. R. Mattaini, J. Yang, K. Hiller, C. M. Jewell,
632 Z. R. Johnson, D. J. Irvine, L. Guarente, J. K. Kelleher, M. G. Vander, Reductive
633 glutamine metabolism by IDH1 mediates lipogenesis under hypoxia. *Nature*. **481**, 380–384
634 (2012).
635 28. M. G. Badur, T. Muthusamy, S. J. Parker, S. Ma, K. Mcbrayer, T. Cordes, J. H. Magana,
636 K. Guan, M. Christian, Oncogenic R132 IDH1 Mutations Limit NADPH for De Novo
637 Lipogenesis through (D)2-Hydroxyglutarate Production in Fibrosarcoma Cells. *Cell Rep.*
638 **25**, 1018–1026 (2018).
639 29. Z. T. Schug, J. Vande Voorde, E. Gottlieb, The metabolic fate of acetate in cancer. *Nat.*

640 *Publ. Gr.* **16**, 708–717 (2016).
641 30. T. Fujino, J. Kondo, M. Ishikawa, K. Morikawa, T. T. Yamamoto, Acetyl-CoA Synthetase
642 2, a Mitochondrial Matrix Enzyme Involved in the Oxidation of Acetate. *J. Biol. Chem.*
643 **276**, 11420–11426 (2001).
644 31. Z. T. Schug, B. Peck, D. T. Jones, Q. Zhang, S. Grosskurth, I. S. Alam, L. M. Goodwin, E.
645 Smethurst, S. Mason, K. Blyth, L. McGarry, D. James, E. Shanks, G. Kalna, R. E.
646 Saunders, M. Jiang, M. Howell, F. Lassailly, M. Z. Thin, B. Spencer-Dene, G. Stamp, N. J.
647 F. van den Broek, G. Mackay, V. Bulusu, J. J. Kamphorst, S. Tardito, D. Strachan, A. L.
648 Harris, E. O. Aboagye, S. E. Critchlow, M. J. O. Wakelam, A. Schulze, E. Gottlieb,
649 Acetyl-CoA synthetase 2 promotes acetate utilization and maintains cancer cell growth
650 under metabolic stress. *Cancer Cell*. **27**, 57–71 (2015).
651 32. S. A. Comerford, Z. Huang, X. Du, Y. Wang, L. Cai, A. K. Witkiewicz, H. Walters, M. N.
652 Tantawy, A. Fu, H. C. Manning, J. D. Horton, R. E. Hammer, S. L. Mcknight, B. P. Tu,
653 Acetate dependence of tumors. *Cell*. **159**, 1591–1602 (2014).
654 33. T. Mashimo, K. Pichumani, V. Vemireddy, K. J. Hatanpaa, D. K. Singh, S. Sirasanagandla,
655 S. Nannepaga, S. G. Piccirillo, Z. Kovacs, C. Foong, Z. Huang, S. Barnett, B. E. Mickey,
656 R. J. Deberardinis, B. P. Tu, E. A. Maher, R. M. Bachoo, Acetate is a bioenergetic
657 substrate for human glioblastoma and brain metastases. *Cell*. **159**, 1603–1614 (2014).
658 34. J. J. Kamphorst, M. K. Chung, J. Fan, J. D. Rabinowitz, Quantitative analysis of acetyl-
659 CoA production in hypoxic cancer cells reveals substantial contribution from acetate.
660 *Cancer Metab.* **2**, 23 (2014).
661 35. B. Yenilmez, M. Kelly, G. Zhang, N. Wetoska, O. R. Ilkayeva, K. Min, L. Rowland, C.
662 DiMarzio, W. He, N. Raymond, L. Lifshitz, M. Pan, X. Han, J. Xie, R. H. Friedline, J. K.
663 Kim, G. Gao, M. A. Herman, C. B. Newgard, M. P. Czech, Paradoxical activation of
664 transcription factor SREBP1c and de novo lipogenesis by hepatocyte-selective ATP-citrate
665 lyase depletion in obese mice. *J. Biol. Chem.*, 102401 (2022).
666 36. S. Zhao, A. M. Torres, R. A. Henry, S. Trefely, M. Wallace, J. V Lee, A. Carrer, A.
667 Sengupta, S. L. Campbell, Y. M. Kuo, A. J. Frey, N. Meurs, J. M. Viola, I. A. Blair, A. M.
668 Weljie, C. M. Metallo, N. W. Snyder, A. J. Andrews, K. E. Wellen, ATP-Citrate Lyase
669 Controls a Glucose-to-Acetate Metabolic Switch. *Cell Rep.* **17**, 1037–1052 (2016).
670 37. F. Bian, T. Kasumov, K. K. Thomas, K. A. Jobbins, F. David, P. E. Minkler, C. L. Hoppel,
671 H. Brunengraber, Peroxisomal and mitochondrial oxidation of fatty acids in the heart,
672 assessed from the 13C labeling of malonyl-CoA and the acetyl moiety of citrate. *J. Biol.*
673 *Chem.* **280**, 9265–9271 (2005).
674 38. A. E. Reszko, T. Kasumov, F. David, K. A. Jobbins, K. R. Thomas, C. L. Hoppel, H.
675 Brunengraber, C. Des Rosiers, Peroxisomal Fatty Acid Oxidation Is a Substantial Source of
676 the Acetyl Moiety of Malonyl-CoA in Rat Heart. *J. Biol. Chem.* **279**, 19574–19579 (2004).
677 39. T. Kasumov, J. E. Adams, F. Bian, F. David, K. R. Thomas, K. A. Jobbins, P. E. Minkler,
678 C. L. Hoppel, H. Brunengraber, Probing peroxisomal β-oxidation and the labelling of
679 acetyl-CoA proxies with [1-13C]octanoate and [3-13C]octanoate in the perfused rat liver.
680 *Biochem. J.* **389**, 397–401 (2005).
681 40. A. He, X. Chen, M. Tan, Y. Chen, D. Lu, X. Zhang, J. M. Dean, B. Razani, I. J. Lodhi,
682 Acetyl-CoA Derived from Hepatic Peroxisomal $β$-Oxidation Inhibits Autophagy and
683 Promotes Steatosis via mTORC1 Activation. *Mol. Cell*. **79**, 30–42 (2020).
684 41. S. Zha, S. Ferdinandusse, J. L. Hicks, S. Denis, T. A. Dunn, R. J. Wanders, J. Luo, A. M.
685 De Marzo, W. B. Isaacs, Peroxisomal branched chain fatty acid β-oxidation pathway is
686 upregulated in prostate cancer. *Prostate*. **63** (2005), pp. 316–323.
687 42. L. Jiang, A. A. Shestov, P. Swain, C. Yang, S. J. Parker, Q. A. Wang, L. S. Terada, N. D.
688 Adams, M. T. Mccabe, B. Pietrak, S. Schmidt, C. M. Metallo, B. P. Dranka, B. Schwartz,
689 R. J. Deberardinis, Reductive carboxylation supports redox homeostasis during anchorage-

690 independent growth. *Nature*. **532**, 255–258 (2016).
691 43. J. Son, C. A. Lyssiotis, H. Ying, X. Wang, S. Hua, M. Ligorio, R. M. Perera, C. R. Ferrone,
692 E. Mullarky, N. Shyh-Chang, Y. Kang, J. B. Fleming, N. Bardeesy, J. M. Asara, M. C.
693 Haigis, R. A. Depinho, L. C. Cantley, A. C. Kimmelman, Glutamine supports pancreatic
694 cancer growth through a KRAS-regulated metabolic pathway. *Nature*. **496**, 101–105
695 (2013).
696 44. A. Kumar, T. Cordes, A. E. Thalacker-Mercer, A. M. Pajor, A. N. Murphy, C. M. Metallo,
697 NaCT/SLC13A5 facilitates citrate import and metabolism under nutrient-limited
698 conditions. *Cell Rep.* **36**, 109701 (2021).
699 45. X. Gao, S. Lin, F. Ren, J. Li, J. Chen, C. Yao, H. Yang, S. Jiang, G. Yan, D. Wang, Y.
700 Wang, Y. Liu, Z. Cai, Y. Xu, J. Chen, W. Yu, P. Yang, Q. Lei, Acetate functions as an
701 epigenetic metabolite to promote lipid synthesis under hypoxia. *Nat. Commun.* **7**, 1–14
702 (2016).
703 46. W. S. Yang, K. J. Kim, M. M. Gaschler, M. Patel, M. S. Shchepinov, B. R. Stockwell,
704 Peroxidation of polyunsaturated fatty acids by lipoxygenases drives ferroptosis. *Proc. Natl.*
705 *Acad. Sci. U. S. A.* **113**, E4966--E4975 (2016).
706 47. O. Feron, The many metabolic sources of acetyl-CoA to support histone acetylation and
707 influence cancer progression. *Ann. Transl. Med.* **7**, S277--S277 (2019).
708 48. M. Wallace, C. R. Green, L. S. Roberts, Y. M. Lee, J. L. McCarville, J. Sanchez-
709 Gurmaches, N. Meurs, J. M. Gengatharan, J. D. Hover, S. A. Phillips, T. P. Ciaraldi, D. A.
710 Guertin, P. Cabrales, J. S. Ayres, D. K. Nomura, R. Loomba, C. M. Metallo, Enzyme
711 promiscuity drives branched-chain fatty acid synthesis in adipose tissues. *Nat. Chem. Biol.*
712 **14**, 1021–1031 (2018).
713 49. L. Izzo1, The carnitine shuttle links mitochondrial metabolism to histone acetylation and
714 lipogenesis. *Co-submitted* (2022).
715 50. X. Liu, D. E. Cooper, A. A. Cluntun, M. O. Warmoes, S. Zhao, M. A. Reid, J. Liu, P. J.
716 Lund, M. Lopes, B. A. Garcia, K. E. Wellen, D. G. Kirsch, J. W. Locasale, Acetate
717 Production from Glucose and Coupling to Mitochondrial Metabolism in Mammals. *Cell*.
718 **175**, 502--513.e13 (2018).
719 51. I. J. Lodhi, C. F. Semenkovich, Peroxisomes: A nexus for lipid metabolism and cellular
720 signaling. *Cell Metab.* **19**, 380–392 (2014).
721 52. O. Apanasets, C. P. Grou, P. P. Van Veldhoven, C. Brees, B. Wang, M. Nordgren, G.
722 Dodt, J. E. Azevedo, M. Fransen, PEX5, the Shuttling Import Receptor for Peroxisomal
723 Matrix Proteins, Is a Redox-Sensitive Protein. *Traffic*. **15**, 94–103 (2014).
724 53. C. Van den Branden, F. Roels, Thioridazine: a selective inhibitor of peroxisomal β-
725 oxidation in vivo. *FEBS Lett.* **187**, 331–333 (1985).
726 54. R. Shi, Y. Zhang, Y. Shi, S. Shi, L. Jiang, Inhibition of peroxisomal β-oxidation by
727 thioridazine increases the amount of VLCFAs and Aβ generation in the rat brain. *Neurosci.*
728 *Lett.* **528**, 6–10 (2012).
729 55. R. J. A. Wanders, H. R. Waterham, S. Ferdinandusse, Metabolic interplay between
730 peroxisomes and other subcellular organelles including mitochondria and the endoplasmic
731 reticulum. *Front. Cell Dev. Biol.* **3**, 1–15 (2016).
732 56. B. S. Jakobs, R. J. A. Wanders, Fatty acid $β$-oxidation in peroxisomes and mitochondria:
733 The first, unequivocal evidence for the involvement of carnitine in shuttling propionyl-
734 CoA from peroxisomes to mitochondria. *Biochem. Biophys. Res. Commun.* **213** (1995), pp.
735 1035–1041.
736 57. F. Leighton, S. Bergseth, T. Rortveit, E. N. Christiansen, J. Bremer, Free acetate
737 production by rat hepatocytes during peroxisomal fatty acid and dicarboxylic acid
738 oxidation. *J. Biol. Chem.* **264**, 10347–10350 (1989).
739 58. A. Carrer, S. Trefely, S. Zhao, S. L. Campbell, R. J. Norgard, K. C. Schultz, S. Sidoli, J. L.

740 D. Parris, H. C. Affronti, S. Sivanand, S. Egolf, Y. Sela, M. Trizzino, A. Gardini, B. A.
741 Garcia, N. W. Snyder, B. Z. Stanger, K. E. Wellen, Acetyl-CoA metabolism supports
742 multistep pancreatic tumorigenesis. *Cancer Discov.* **9**, 416–435 (2019).
743 59. J. M. Bae, J. H. Kim, H. J. Oh, H. E. Park, T. H. Lee, N. Cho, G. H. Kang, Downregulation
744 of acetyl-CoA synthetase 2 is a metabolic hallmark of tumor progression and
745 aggressiveness in colorectal carcinoma. **30**, 267–277 (2016).
746 60. V. Bulusu, S. Tumanov, E. Michalopoulou, N. J. Van Den Broek, G. Mackay, C. Nixon, S.
747 Dhayade, Z. T. Schug, J. Vande Voorde, K. Blyth, E. Gottlieb, A. Vazquez, J. J.
748 Kamphorst, Acetate Recapturing by Nuclear Acetyl-CoA Synthetase 2 Prevents Loss of
749 Histone Acetylation during Oxygen and Serum Limitation Article Acetate Recapturing by
750 Nuclear Acetyl-CoA Synthetase 2 Prevents Loss of Histone Acetylation during Oxygen
751 and Serum Limi. *Cell Rep.* **18**, 647–658 (2017).
752 61. L. Yao, L. Jiang, F. Zhang, M. Li, B. Yang, F. Zhang, X. Guo, Acetate promotes SNAI1
753 expression by ACSS2-mediated histone acetylation under glucose limitation in renal cell
754 carcinoma cell. *Biosci. Rep.* **40**, 1–10 (2020).
755 62. S. Trefely, C. D. Lovell, N. W. Snyder, K. E. Wellen, Compartmentalised acyl-CoA
756 metabolism and roles in chromatin regulation. *Mol. Metab.* **38**, 100941 (2020).
757 63. A. Luengo, D. Y. Gui, M. G. Vander Heiden, Targeting Metabolism for Cancer Therapy.
758 *Cell Chem. Biol.* **24**, 1161–1180 (2017).
759 64. C. W. T. Van Roermund, E. H. Hettema, M. Van Den Berg, H. F. Tabak, R. J. A. Wanders,
760 Molecular characterization of carnitine-dependent transport of acetyl-CoA from
761 peroxisomes to mitochondria in Saccharomyces cerevisiae and identification of a plasma
762 membrane carnitine transporter, Agp2p. *EMBO J.* **18**, 5843–5852 (1999).
763 65. S. M. Houten, R. J. A. Wanders, P. Ranea-Robles, Metabolic interactions between
764 peroxisomes and mitochondria with a special focus on acylcarnitine metabolism. *Biochim.*
765 *Biophys. Acta - Mol. Basis Dis.* **1866**, 165720 (2020).
766 66. J. D. Young, INCA: A computational platform for isotopically non-stationary metabolic
767 flux analysis. *Bioinformatics*. **30**, 1333–1335 (2014).
768 67. T. Cordes, C. M. Metallo, "Quantifying Intermediary Metabolism and Lipogenesis in
769 Cultured Mammalian Cells Using Stable Isotope Tracing and Mass Spectrometry" in *High-*
770 *Throughput Metabolomics: Methods and Protocols*, A. D'Alessandro, Ed. (Springer New
771 York, New York, NY, 2019; https://doi.org/10.1007/978-1-4939-9236-2_14), pp. 219–241.
772 68. F. A. Ran, P. D. Hsu, J. Wright, V. Agarwala, D. A. Scott, F. Zhang, Genome engineering
773 using the CRISPR-Cas9 system. *Nat. Protoc.* **8**, 2281–2308 (2013).
774 69. N. E. Sanjana, O. Shalem, F. Zhang, Improved vectors and genome-wide libraries for
775 CRISPR screening. *Nat. Methods*. **11**, 783–784 (2014).
776 70. S. Kim, D. Kim, S. W. Cho, J. Kim, J. S. Kim, Highly efficient RNA-guided genome
777 editing in human cells via delivery of purified Cas9 ribonucleoproteins. *Genome Res.* **24**,
778 1012–1019 (2014).
779 71. A. Kumar, J. Mitchener, Z. A. King, C. M. Metallo, Escher-Trace: A web application for
780 pathway-based visualization of stable isotope tracing data. *BMC Bioinformatics*. **21**, 1–10
781 (2020).
782

783 **Acknowledgments**

784

785 We thank all members of the Metallo laboratory for support and helpful discussions.
786 ACLY and ACSS2 cellular reagents were provided by Nimbus Therapeutics. Figure
787 panels were made with Biorender. **Funding:** US National Institutes of Health (NIH)
788 grants R35CA220538 and P01CA120964 (to R.J.S.) and R01CA234245 (to C.M.M.).

A.K. was supported in part by U54CA132379, and H.G. was supported in part by T32DK007541.

Author contributions: A.K., R.K., R.U.S. and C.M.M. conceived and designed the study. A.K. and R.K. performed experiments. R.K. generated the *PEX5*-KO cell lines. H.G. and R.J.S. provided 643T cell lines and advised on studies. G.H.M. and C.R.G. performed LC-MS/MS lipidomic analytics. T.C. performed the ferroptosis assay. A.K., R.K. and C.M.M wrote the paper with input from all authors. **Competing interests:** Robert Svensson is an employee of Nimbus Therapeutics. Christian Metallo is a scientific advisor for Faeth Therapeutics. **Data and materials availability:** This study did not generate new unique reagents. The datasets supporting the current study are available from the corresponding author upon request.

Figures and Tables

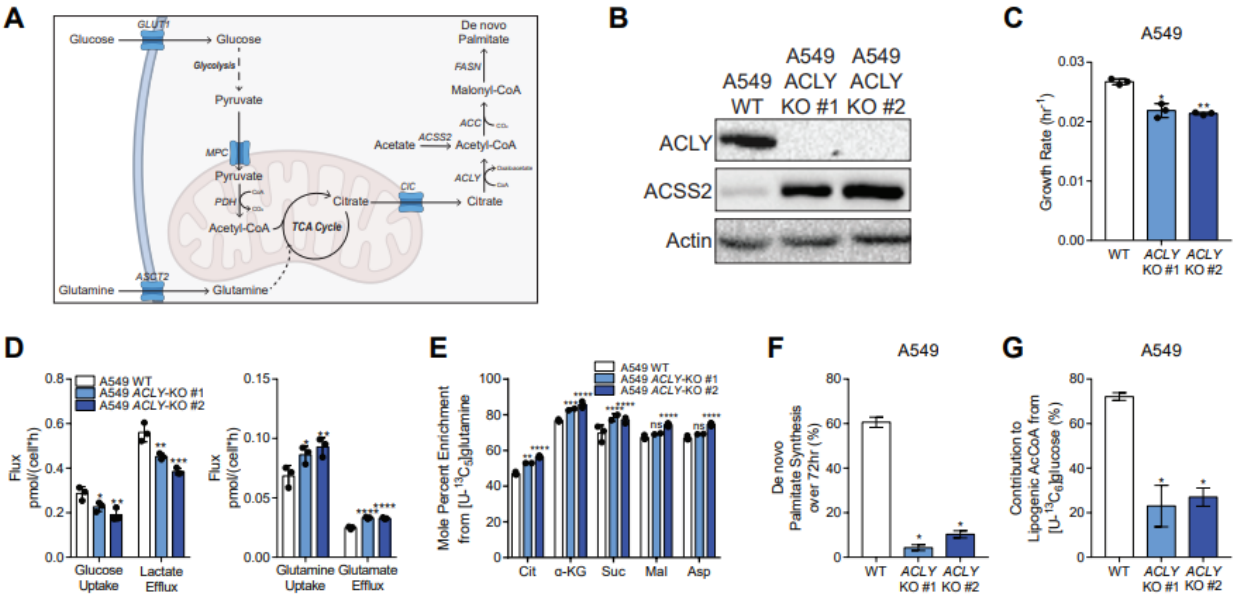

Fig. 1. *ACLY*-KO rewires central carbon metabolism and leads to a reduction of palmitate synthesis in cancer cells

(A) The pyruvate-citrate shuttle and fatty acid synthesis.

(B) Western Blots of ACLY, ACSS2, and actin in A549 WT and *ACLY*-KO cells.

(C) Growth rates of A549 WT and *ACLY*-KO cells grown in high glucose DMEM +10% FBS for 4 days.

(D) Glucose uptake, lactate efflux (left) and glutamine uptake, glutamate efflux (right) in A549 WT and *ACLY*-KO cells cultured in high glucose DMEM +10% dFBS for 72 hours (n=3).

(E) Mole percent enrichment of TCA intermediates from [U-$^{13}C_5$]glutamine in A549 *ACLY*-KO clones cultured in high glucose DMEM +10% dFBS for 72 hours (n=3).

(F) De novo synthesis of palmitate in A549 *ACLY*-KO cells cultured in [U-$^{13}C_6$]glucose +10% dFBS for 72 hours (n=3).

(G) Percent of lipogenic acetyl-CoA contributed by [U-$^{13}C_6$]glucose in A549 *ACLY*-KO cells cultured in high glucose DMEM +10% dFBS 72 hours (n=3).

In (C-G) data are plotted as mean ± SD. Statistical significance is relative to WT as determined by One-way ANOVA w/ Dunnet's method for multiple comparisons (C-E) with *, P value < 0.05; **, P value < 0.01; ***, P value < 0.001, ****, P value < 0.0001. In (F,G) data are plotted as mean ± 95% confidence interval (CI). Statistical significance by non-overlapping confidence intervals, *. Unless indicated, all data represent biological triplicates. Data shown are from one of at least two separate experiments. See also Figure S1.

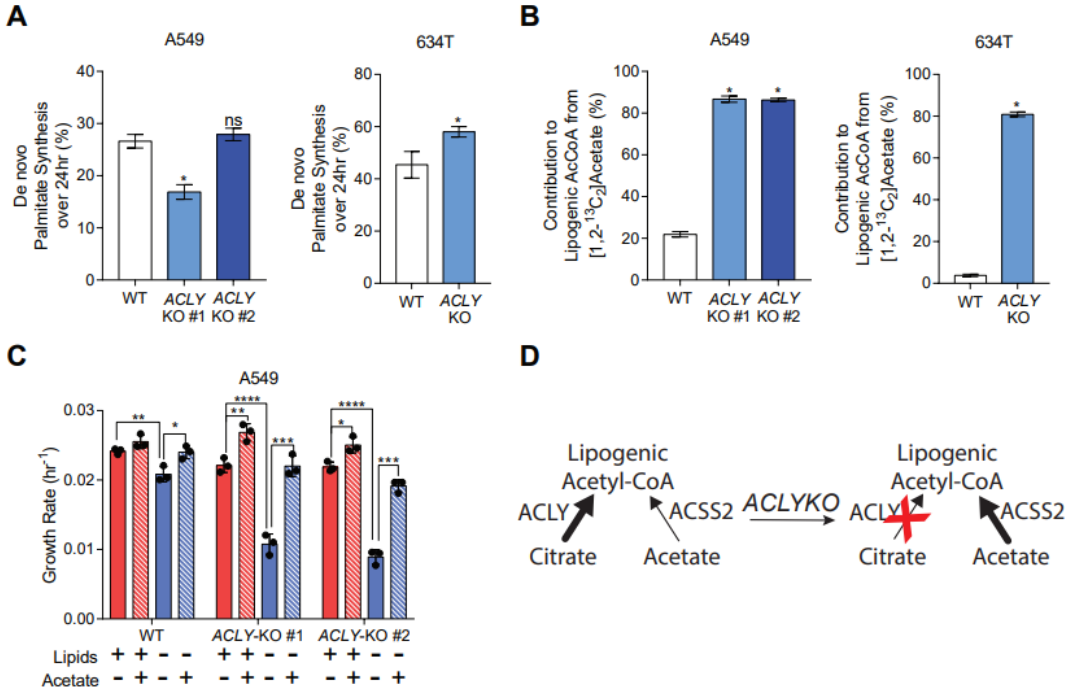

Fig. 2. *ACLY*-KO growth and fatty acid synthesis is rescued with addition of extracellular acetate

(A) De novo synthesis of palmitate in A549 (left) and 634T (right) WT and *ACLY*-KO cells cultured in high glucose DMEM +10% dFBS + 1 mM acetate for 24 hours (n=3).

(B) Percent of lipogenic acetyl-CoA contributed by [1,2-$^{13}C_2$]acetate in A549 (left) and 634T (right) and *ACLY*-KO cells cultured in high glucose DMEM +10% dFBS + 1 mM acetate for 24 hours (n=3).

(C) Growth rates of A549 WT and *ACLY*-KO cells grown in high glucose DMEM +10% dFBS or delipidated dFBS +/- 1 mM acetate for 4 days (n=3).

(D) Schematic of lipogenic acetyl-CoA synthesis in *ACLY*-KO cells.

In (A,B) data are plotted as mean ± 95% confidence interval (CI). Statistical significance by non-overlapping confidence intervals, *. In (C) data are plotted as mean ± SD. Statistical significance is determined by Two-way ANOVA w/ Tukey's method for multiple comparisons with *, P value < 0.05; **, P value < 0.01; ***, P value < 0.001, ****, P value < 0.0001. Unless indicated, all data represent biological triplicates. Data shown are from one of at least two separate experiments. See also Figure S2.

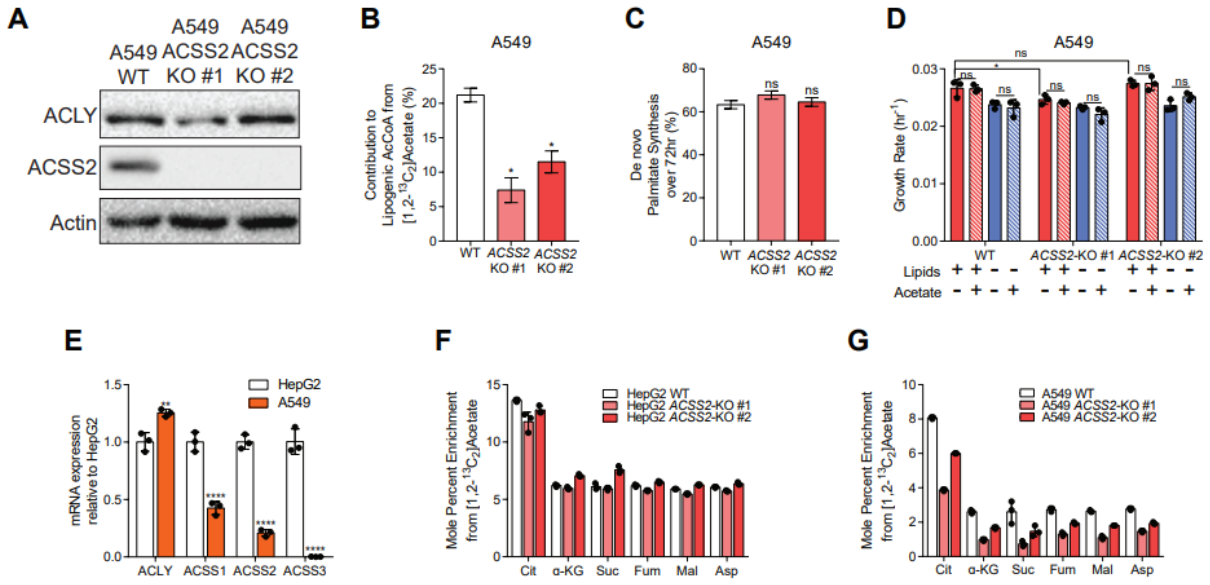

Fig. 3. *ACSS2*-KO attenuates catabolism of exogenous acetate with minimal effect on glucose catabolism

(A) Western Blots of ACLY, ACSS2, and actin in A549 WT and *ACSS2*-KO cells.
(B) Percent of lipogenic acetyl-CoA contributed by [1,2-$^{13}C_2$] acetate in A549 *ACSS2*-KO cells cultured in high glucose DMEM +10% dFBS + 1 mM acetate for 24 hours (n=3).
(C) De novo synthesis of palmitate in A549 *ACSS2*-KO cells cultured in high glucose DMEM +10% dFBS for 72 hours (n=3).
(D) Growth rates of A549 WT and *ACSS2*-KO cells grown in high glucose DMEM +10% dFBS or delipidated dFBS +/- 1 mM acetate for 4 days (n=3).
(E) mRNA expression of acetyl-CoA generating enzymes in HepG2 and A549 cells (n=3).
(F) Mole percent enrichment of TCA intermediates from [1,2-$^{13}C_2$] acetate in HepG2 *ACSS2*-KO cells cultured in high glucose DMEM +10% dFBS + 1 mM acetate for 24 hours (n=3).
(G) Mole percent enrichment of TCA intermediates from [1,2-$^{13}C_2$] acetate in A549 *ACSS2*-KO cells cultured in high glucose DMEM +10% dFBS + 1 mM acetate for 24 hours (n=3).
In (B, C) data are plotted as mean ± 95% confidence interval (CI). Statistical significance by non-overlapping confidence intervals, *. In (D-G) data are plotted as mean ± SD. Statistical significance is determined by Two-way ANOVA w/ Tukey's method for multiple comparisons (D); or relative to HepG2 as determined by two-sided Student's t-test (G) with *, P value < 0.05; **, P value < 0.01; ***, P value < 0.001, ****, P value < 0.0001. Unless indicated, all data represent biological triplicates. Data shown are from one of at least two separate experiments. See also Figure S3.

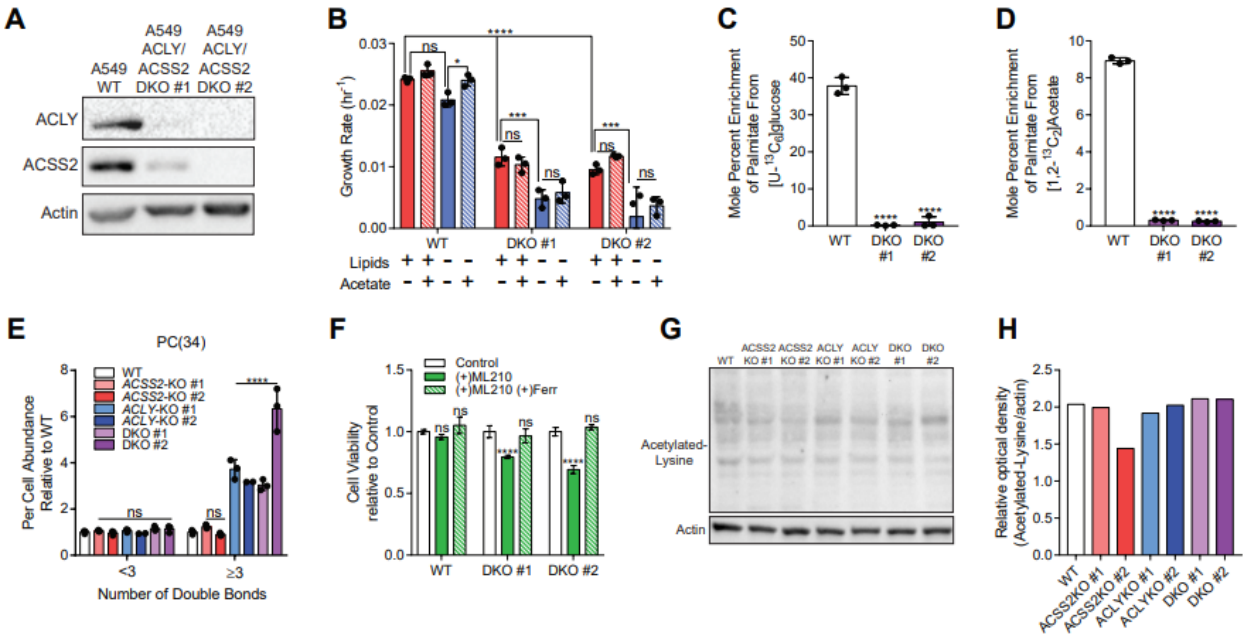

Fig. 4. *ACLY/ACSS2*-DKO cells are reliant on extracellular lipids, with minimal change in protein acetylation.

(A) Western Blots of ACLY, ACSS2, and actin in A549 WT and *ACLY/ACSS2*-DKO cells.

(B) Growth rates of A549 WT and *ACLY/ACSS2*-DKO cells grown in high glucose DMEM +10% dFBS or delipidated dFBS +/- 1 mM acetate for 4 days (n=3).

(C) Mole percent enrichment of palmitate from [U-$^{13}C_6$] glucose in A549 *ACLY/ACSS2*-DKO cells cultured in high glucose DMEM +10% dFBS for 72 hours (n=3).

(D) Mole percent enrichment of palmitate from [1,2-$^{13}C_2$] acetate in A549 *ACLY/ACSS2*-DKO cells cultured in high glucose DMEM +10% dFBS + 1 mM acetate for 24 hours (n=3).

(E) PC(34) abundance of A549 WT, ACSS2-KO, ACLY-KO, ACLY/ACSS2-DKO cells cultured in high glucose DMEM +10% FBS for 2 days (n=3).

(F) Cell viability of A549 WT and ACLY/ACSS2-DKO cells cultured in DMEM+10% dFBS +/- 2 µM ML210 and/or 2 µM Ferrostatin for 48 hours (n=4).

(G) Western Blots of acetylated-lysine and actin in A549 WT, ACSS2-KO, ACLY-KO, ACLY/ACSS2 DKO whole cell lysates.

(H) Relative optical density of acetylated-lysine/actin in A549 WT, ACSS2-KO, ACLY-KO, ACLY/ACSS2-DKO whole cell lysates (n=1).

In (B-F) data are plotted as mean ± SD. Statistical significance is determined by Two-way ANOVA w/ Tukey's method for multiple comparisons (B); or relative to WT as determined by One-way ANOVA w/ Dunnet's method for multiple comparisons (C-F) with *, P value < 0.05; **, P value < 0.01; ***, P value < 0.001, ****, P value < 0.0001. Unless indicated, all data represent biological triplicates. Data shown are from one of at least two separate experiments. See also Figure S4.

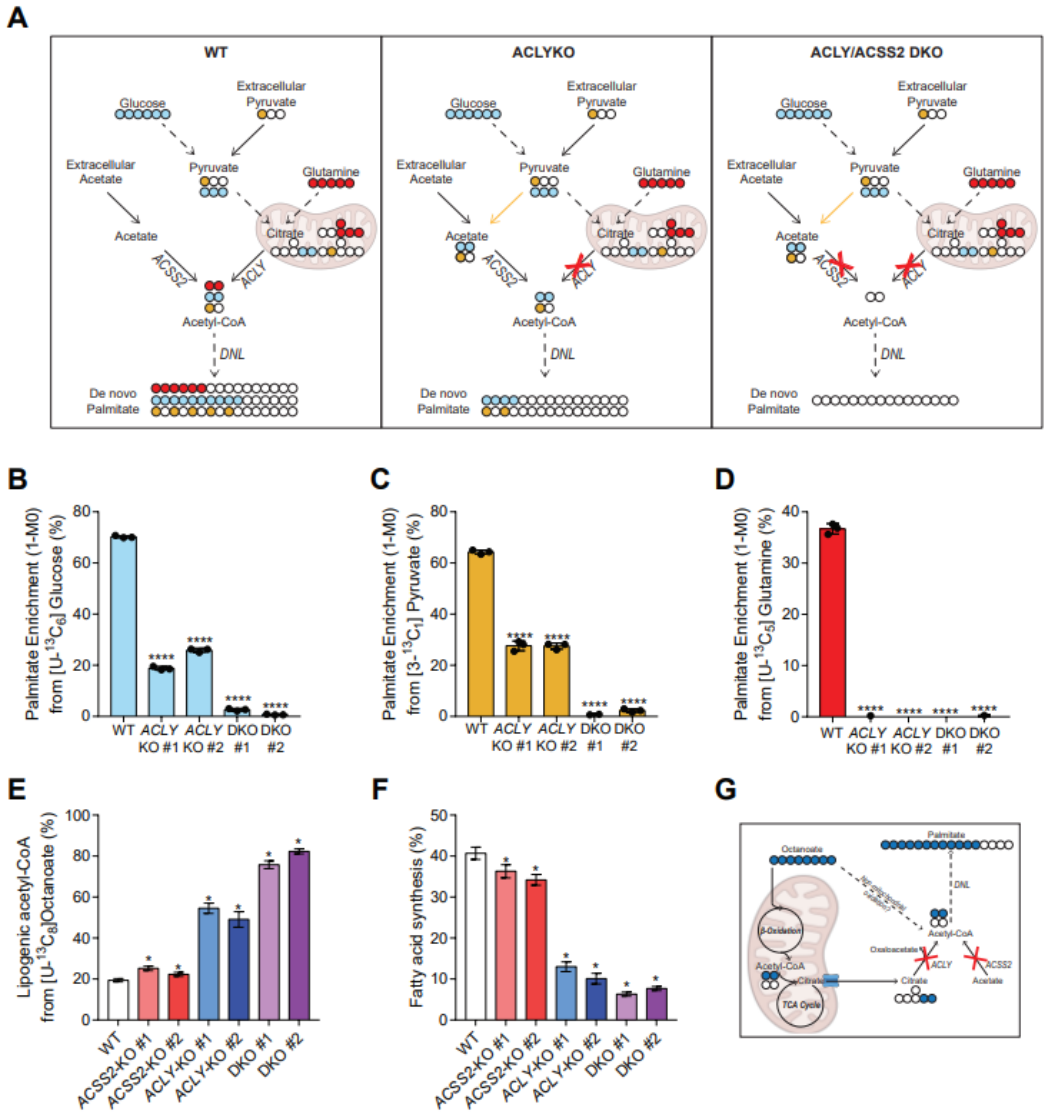

Fig. 5. Disruption of canonical acetyl-CoA synthesis induces alternative synthesis pathways.
(A) Schematic showing de novo acetate synthesis in *ACLY*-KO cells. Dashed lines represent multiple reactions.
(B) Enrichment (1-M0) of palmitate from [U-$^{13}C_6$] glucose in A549 WT, *ACLY*-KO, *ACLY/ACSS2*-DKO cells cultured in high glucose DMEM +10% dFBS for 72 hours (n=3).
(C) Enrichment (1-M0) of palmitate from [3-$^{13}C_1$] pyruvate in A549 WT, *ACLY*-KO, *ACLY/ACSS2*-DKO cells cultured in high glucose DMEM +10% dFBS + 5mM pyruvate for 72 hours (n=3).
(D) Enrichment (1-M0) of palmitate from [U-$^{13}C_5$] glutamine in A549 WT, *ACLY*-KO, *ACLY/ACSS2*-DKO cells cultured in high glucose DMEM +10% dFBS for 72 hours (n=3).
(E) Percent of lipogenic acetyl-CoA contributed by [U-$^{13}C_8$] octanoate in A549 WT, ACSS2-KO, ACLY-KO, ACLY/ACSS2-DKO cells cultured in high glucose DMEM +10% dFBS + 500 µM octanoate for 24 hours (n=3).

(F) De novo synthesis of palmitate in A549 WT, ACSS2-KO, ACLY-KO, ACLY/ACSS2-DKO cells cultured in high glucose DMEM +10% dFBS + 500 µM octanoate for 24 hours (n=3).

(G) Schematic of non-mitochondrial acetyl-CoA synthesis from [U-$^{13}C_8$] octanoate in ACLY/ACSS2-DKO cells. Filled circles are 13C, empty circles are 12C.

In (B-D) data are plotted as mean ± SD. Statistical significance relative to WT as determined by One-way ANOVA w/ Dunnet's method for multiple comparisons (B-F) with *, P value < 0.05; **, P value < 0.01; ***, P value < 0.001, ****, P value < 0.0001. In (F,G) data are plotted as mean ± 95% confidence interval (CI). Statistical significance by non-overlapping confidence intervals, *. Unless indicated, all data represent biological triplicates. Data shown are from one of at least two separate experiments. See also Figure S5.

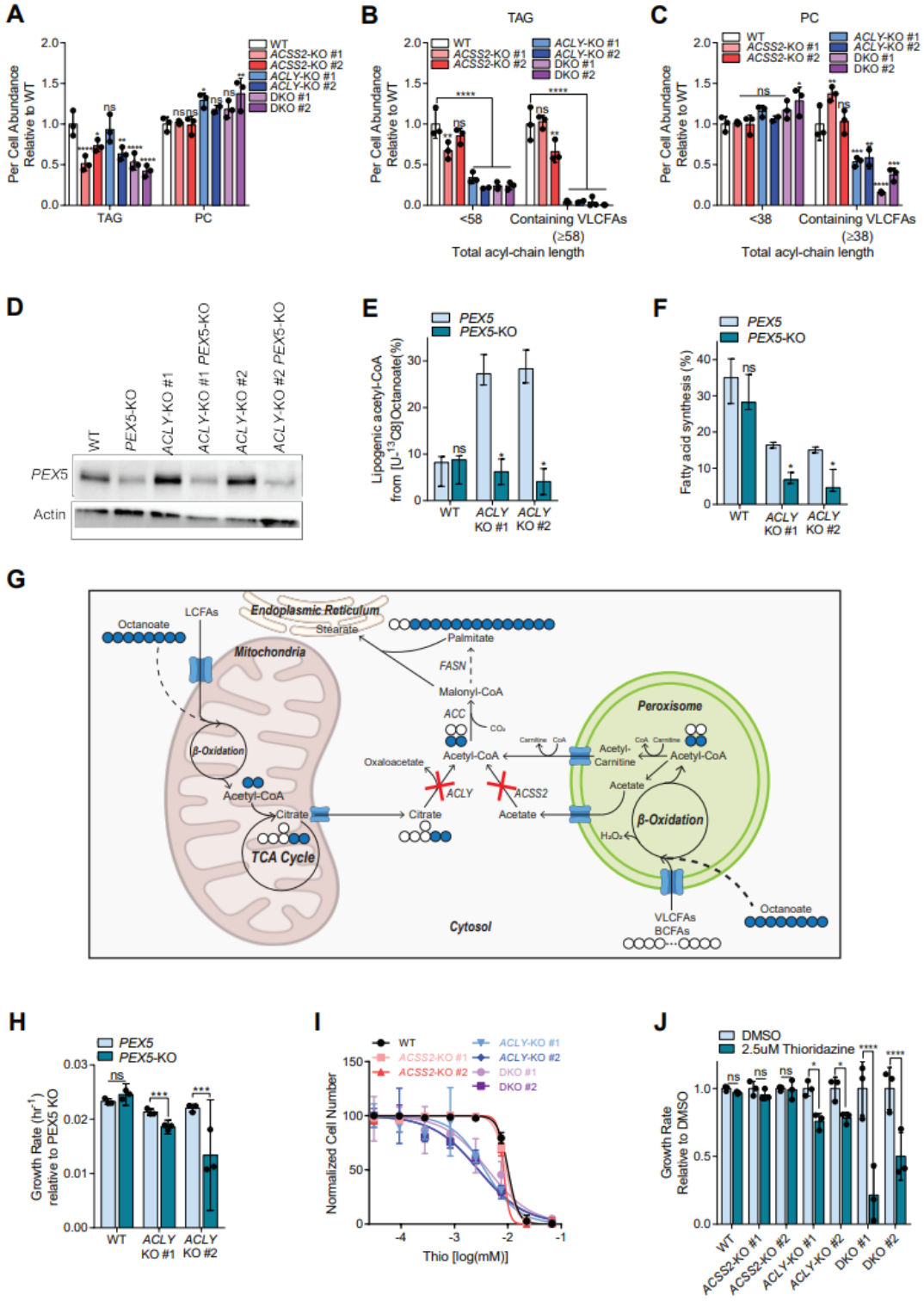

Fig. 6. Peroxisomal β-oxidation becomes a major source of lipogenic acetyl-CoA with ACLYKO and ACLY/ACSS2 DKO.

(A) Total abundance of TAGs and PCs in A549 WT, ACSS2-KO, ACLY-KO, ACLY/ACSS2-DKO cells cultured in high glucose DMEM +10% FBS for 2 days (n=3).

(B) Total abundance of saturated, mono- and di-unsaturated TAGs per cell of A549 WT, ACSS2-KO, ACLY-KO, ACLY/ACSS2-DKO cells cultured in high glucose DMEM +10% FBS for 2 days (n=3).

(C) Total abundance of saturated and monounsaturated PCs per cell of A549 WT, ACSS2-KO, ACLY-KO, ACLY/ACSS2-DKO cells cultured in high glucose DMEM +10% FBS for 2 days (n=3).

(D) Western blots of PEX5 and actin in A549 WT, PEX5 KO, ACLY KO and ACLY-PEX5-KO cells.

(E) Percent of lipogenic acetyl-CoA contributed by [U-$^{13}C_8$]] octanoate in A549 WT, PEX5-KO, ACLY-KO and ACLY/PEX-5 KO cells cultured in high glucose DMEM +10% dFBS for 48 hours (n=3).

(F) De novo synthesis of palmitate in A549 WT, PEX5-KO, ACLY-KO and ACLY/PEX-5 KO cells cultured in high glucose DMEM +10% dFBS for 72 hours (n=3).

(G) Schematic of peroxisomal acetyl-CoA synthesis from [U-$^{13}C_8$] octanoate in *ACLY/ACSS2*-DKO cells. Filled circles are 13C, empty circles are 12C.

(H) Growth rates of A549 WT and ACLY-KO relative to PEX5 KO cells grown in high glucose DMEM +10% FBS for 4 days.

(I) Dose response of A549 WT, *ACSS2*-KO, *ACLY*-KO, *ACLY/ACSS2*-DKO cells cultured in high glucose DMEM +10% dFBS to Thioridazine over 4 days (n=3).

(J) Growth rates of A549 WT and ACLY/ACSS2-DKO cells grown in high glucose DMEM +10% dFBS +/- 2.5 μM thioridazine relative to DMSO for 4 days (n=3).

In (A-C, H, J) data are plotted as mean ± SD. Statistical significance as determined by One-way ANOVA w/ Dunnet's method for multiple comparisons relative to WT (A-C) or DMSO (J) with *, P value < 0.05; **, P value < 0.01; ***, P value < 0.001, ****, P value < 0.0001. In (E,F) data are plotted as mean ± 95% confidence interval (CI). Statistical significance by non-overlapping confidence intervals, *.
Unless indicated, all data represent biological triplicates. Data shown are from one of at least two separate experiments. See also Figure S6.

Table 1. Key Resources Table

REAGENT or RESOURCE	SOURCE	IDENTIFIER

Bacterial and virus strains		
One Shot Stbl3 E. Coli	ThermoFisher Scientific	Cat#C7373
Library Efficiency DH5α Competent Cells	ThermoFisher Scientific	Cat#18263012
Chemicals, peptides, and recombinant proteins		
[U-$^{13}C_6$] Glucose	Cambridge Isotope Labs	Cat#CLM-1396
[U-$^{13}C_5$] Glutamine	Cambridge Isotope Labs	Cat#CLM-1822
[U-$^{13}C_2$] Acetate	Cambridge Isotope Labs	
[3-$^{13}C_1$] Pyruvate	Cambridge Isotope Labs	
[2,4-$^{13}C_6$] Citrate	Cambridge Isotope Labs	Cat#CLM-148
[U-$^{13}C_8$] Octanoate	Cambridge Isotope Labs	Cat#CLM-9617
MTBSTFA + 1% TBDMSCl	Regis Technologies	Cat#1-270143-200
BsmBI	New England Biolabs	Cat#R0580L
Critical commercial assays		
Lipofectamine 3000	ThermoFisher Scientific	Cat#L3000008
KAPA HiFi HotStart Ready Mix	Kapa Biosystems	Cat#KK2602
iTaq Universal SYBR Green	Biorad	Cat#1725121
iScript Reverse Transcription Supermix	Biorad	Cat#1708840
RNeasy Mini Kit	QIAGEN	Cat#74104
Zero Blunt TOPO PCR Cloning Kit	ThermoFisher Scientific	Cat#450245
prepGEM gold buffer	Zygem	
Experimental models: cell lines		
HepG2	ATCC	Cat#HB-8065
A549	ATCC	Cat#CCL-185
HAP1	Horizon Discovery	Cat#C631
634T	Svensson et. al. (2016)	NA
HEK293FT	ThermoFisher Scientific	Cat#R70007
Oligonucleotides		
See Table S1		
Recombinant DNA		
LentiCRISPR v2 plasmid	Addgene	Cat#52961
pCMVR8.2	Addgene	Cat#12263
pMD2.G	Addgene	Cat#12259
Software and algorithms		
MATLAB 2016b	MathWorks	https://www.mathworks.com/products/matlab.html
Escher-Trace	Kumar et al. (2020)	https://escher-trace.github.io/
GraphPad Prism 7.00	GraphPad	https://www.graphpad.com/scientific-software/prism/
INCA	Young et al. (2014)	https://mfa.vueinnovations.com/
CRISPOR	Concordet et al. (2018)	http://crispor.tefor.net/
NCBI BLAST	Agarwala et al. (2018)	https://blast.ncbi.nlm.nih.gov/